Available online at www.sciencedirect.com
ScienceDirect
Trans. Nonferrous Met. Soc. China 35(2025) 1406−1423
Transactions of Nonferrous Metals Society of China
www.tnmsc.cn

Fungal corrosion behavior and mechanism of deposit-covered aluminum alloy 7075 in marine environment

Jia-ping WANG[1], Yi ZHANG[2], Hong-wei LIU[1], Yan-sheng YIN[2]

1. School of Chemical Engineering and Technology, Sun Yat-sen University, Zhuhai 519082, China;
2. Guangdong Key Laboratory of Materials and Equipment in Harsh Marine Environment, Guangzhou Maritime University, Guangzhou 510725, China

Received 5 September 2023; accepted 21 May 2024

Abstract: The corrosion behavior of deposit-covered aluminum alloy 7075 (AA7075) caused by fungus *Aspergillus terreus* (*A. terreus*) was thoroughly investigated in artificial seawater aiming to offer some new insights into the under-deposit corrosion mechanism of aluminum alloys in marine environments containing fungi. Electrochemical impedance spectroscopy, polarization curves, wire beam electrodes, and surface analysis were performed. Results indicate that *A. terreus* can survive beneath the deposit but the counts of sessile spores decline as the increase of deposit thickness, suggesting a poor biological activity of *A. terreus* beneath the deposit. Both the uniform corrosion and pitting corrosion are accelerated by *A. terreus*, while the pitting corrosion of AA7075 alloys beneath the deposit derives from a galvanic cell with a small anode and a large cathode. Deposits have a corrosion inhibition effect on AA7075. However, the galvanic effect caused by the bare and deposit-covered AA specimens is obviously enhanced by *A. terreus*.
Key words: fungal corrosion; under-deposit corrosion; pitting corrosion; *Aspergillus terreus*; aluminum alloy 7075

1 Introduction

Aluminum alloys (AAs) have widely practical applications in offshore structures owing to their superior versatility of high strength, good machining properties, and low density [1]. The mechanical and anti-corrosion performances of AAs have been quickly improved with the development of smelting, forging, and welding processes, and they reach or even surpass traditional metal materials, such as carbon steels [2−4]. Nowadays, different types of AAs are flexibly employed in specific areas according to their actual demands, such as superstructures, submarine pipelines, and offshore operating platforms. However, AA easily suffers from severe localized corrosion, especially in highly corrosive marine environments, and pitting corrosion [5], stress corrosion [6], and microbiologically influenced corrosion (MIC) [7,8] are primary.

MIC dominates a significant position in all corrosion types, and more than 20% of economic losses induced by corrosion are related to MIC [9,10]. MIC is a complex electrochemical corrosion, and many microorganisms, including bacteria and fungi, can be involved in the whole corrosion process [11−14]. Microorganisms can directly or indirectly accelerate metal corrosion, and the direct way is related to the direct electron from metal to microorganisms while the indirect way is attributed to metabolic products secreted by microorganisms, such as the extracellular polymeric substances (EPS) [15,16]. Recently, most MIC studies have

Corresponding author: Hong-wei LIU, Tel: +86-18826212630, E-mail: liuhw35@mail.sysu.edu.cn;
Yan-sheng YIN, Tel: +86-15921626693, E-mail: ysyin@shmtu.edu.cn
https://doi.org/10.1016/S1003-6326(24)66757-9

predominantly focused on bacteria, but fungi also exhibit notable corrosive properties particularly on AAs, resulting in severe localized corrosion. Fungal spores are widely distributed in the natural environment, and they can attach to metal surface and survive well. Furthermore, fungi can easily enhance the formation of defects in AA passive film by modifying its structure [17,18]. However, the fungal corrosion behavior and mechanism of AA, particularly in marine environment, remain unclear due to the limited studies.

It can be speculated that fungal corrosion behavior will be complicated and changeable if some deposits participate in the whole corrosion process. Under natural conditions, some deposits, such as soil and sand, can readily accumulate on equipment materials, causing under-deposit corrosion (UDC) [19]. UDC typically leads to localized corrosion due to the formation of a galvanic-couple cell triggered by the presence of deposits [20]. The presence of microorganisms will affect UDC. SUAREZ et al [21] found that microbial consortium could deeply affect the corrosion behavior of the sand-deposited and sand-free metal, leading to higher corrosion rates. It has been previously reported that a significant UDC acceleration is derived from the enhancement effect of sulfate-reducing bacteria (SRB) [22]. The previous investigation [23] demonstrated that *Pseudomonas stutzeri* could inhibit the galvanic corrosion between the bare and deposit-covered steel specimens by decreasing their galvanic effect. Furthermore, some studies proposed that some specific deposits could hinder corrosion by preventing the migration of corrosion ions and dissolved oxygen from the solution to the solid−liquid interface [24−26]. Hence, the corrosion behavior and mechanism of AAs will undergo significant changes when fungi coexist with deposits. However, the related corrosion studies are poor.

In this work, fungal corrosion of deposit-covered AA7075 with different thicknesses in artificial seawater containing fungus *Aspergillus terreus* (*A. terreus*) was deeply investigated. Surface analysis was performed to characterize the morphology and composition of the corrosion products. Electrochemical measurements were conducted to analyze corrosion behavior and mechanism. The galvanic corrosion between the deposit-covered and bare AA7075 was also studied based on galvanic current density and wire beam electrode (WBE) to explore the influence of *A. terreus*. This study aims to give a comprehensive understanding of under-deposit corrosion of AA7075 caused by fungi.

2 Experimental

2.1 Preparation of AA7075 specimens

AA7075 with a high-strength was selected in this work, and its chemical composition (wt.%) was: 2.40 Mg, 6.00 Zn, 2.50 Cu, 0.40 Si, 0.50 Fe, 0.30 Mn, 0.18 Cr, 0.20 Ti, and Al balance. The working electrodes had a size of 10 mm × 10 mm × 10 mm with a working face of 1 cm^2. Specimens of 20 mm × 10 mm × 5 mm were applied to surface analysis. All the specimens were mechanically polished with grit silicon carbide papers of $400^{\#}$, $600^{\#}$, $800^{\#}$, and $1200^{\#}$ in series. Subsequently, the polished specimens were cleaned with deionized water, acetone, and ethanol, respectively. Last, the cleaned specimens were dried using N_2. Before tests, the specimens were sterilized by ultraviolet radiation for over 30 min.

2.2 Fungal cultivation and inoculation

A. terreus, one of the typical fungi, was isolated from the South China Sea [27]. *A. terreus* was cultured in a potato dextrose liquid medium containing 30 g/L NaCl, 20 g/L dextrose, and 200 g/L potato infusion. Before inoculation, the fresh medium was first sterilized at 121 °C for over 20 min. *A. terreus* was cultured at 37 °C after inoculation. Both the planktonic and sessile spores of *A. terreus* were quantitatively counted based on a spread plate method.

2.3 Test solution and deposits

According to the standard of ASTMD 1141—98, the test solution, i.e., artificial seawater, was prepared, and its chemical composition could be found in a previous study [27]. To improve the biological activity of *A. terreus*, 10 wt.% culture medium of *A. terreus* was added to the artificial seawater. The test solution was also sterilized at 121 °C for more than 20 min. The deposits were composed of sand and clay with a mass ratio of 5:1. The sand has a small size of less than 0.4 mm. The deposits were sterilized at 150 °C in a drying oven

for 1 h. The deposit thicknesses covered on the specimen surface were 0, 1, 3, and 6 mm, respectively.

2.4 Characterization of corrosion product film and biofilms

After corrosion tests of 14 d in artificial seawater, the specimens were first taken out. Immediately, the deposits were slightly removed by normal saline solution, and then the specimens were placed in 2.5 wt.% glutaraldehyde solution to fix biofilm with an immersion time of 4 h. Subsequently, the biofilm-covered specimens were dehydrated by ethanol solution with the concentrations of 50%, 70%, 80%, 90%, and 100%, and each immersion was last for 10 min. Then, the specimens were dried in an N_2 atmosphere. Scanning electron microscopy (SEM, JSM-IT200, Japan) from JEOL, energy dispersive X-ray spectroscopy (EDS), and X-ray diffraction (XRD, BrukerAXS, Germany) were conducted to characterize the surface films. A Leica three-dimensional microscope (DVM6, Germany) was used to study the bare localized corrosion morphologies of specimens under different test conditions.

2.5 Electrochemical measurements

A Corrtest workstation (CS350H, Wuhan, China) with a three-electrode cell was used to do electrochemical measurements, and the deposit-covered specimens, saturated calomel electrode (SCE) and platinum plate corresponded to working electrode, reference electrode, and counter electrode, respectively. The electrochemical impedance spectroscopy (EIS) data were measured in a frequency range from 10^5 to 10^{-2} Hz after a stable open circuit potential (OCP). After 14 d of testing, potentiodynamic polarization curves in a potential range from −350 to 550 mV (vs OCP) were scanned, and the sweep rate was 0.5 mV/s. The galvanic current density between bare and deposit-covered electrodes was performed with a Gammy workstation (Reference 3000, USA). The WBE was constructed with 100 pieces of AA7075, and the single electrode had a diameter of 1 mm. The current density distributions of WBE under various test conditions were measured by Corrtest electrochemical instrument (CST520, China). The schematic diagrams of the galvanic current density and WBE measurements are shown in Fig. 1. Each test was repeated at least three times.

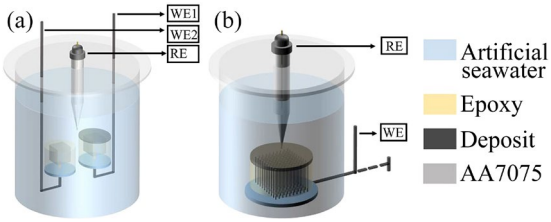

Fig. 1 Schematic diagrams of galvanic current density (a) and WBE (b) measurements (WE: Working electrode; RE: Reference electrode)

3 Results

3.1 Biological activities of *A. terreus*

Figure 2(a) depicts the fungal growth curve in artificial seawater. The initial *A. terreus* spore concentration ($N_{A.terreus}$) is 5.4×10^4 spores/mL, and then *A. terreus* grows fast during the initial 6 d, i.e., logarithmic phase. The spore concentration changes a little from 6 to 12 d corresponding to the stationary phase. Subsequently, the spore counts decline fast with time due to the consumption of nutrients. The sessile *A. terreus* for the specimens covered with different deposit thicknesses are presented in Fig. 2(b). The sessile spores of *A. terreus* decline with the increase of deposit thickness, i.e., the deposit adversely affects the biological activity of sessile *A. terreus*. However, *A. terreus* can survive beneath the deposits, accelerating the corrosion of AA7075. The pH values of the solution under various test conditions on the 14th day are shown in Fig. 2(c). The pH values tend to approach 7 under abiotic conditions, while they are 4−5 in biotic conditions due to *A. terreus*. The decrease in pH values is attributed to the organic acids secreted by *A. terreus*.

3.2 Morphologies of surface films

Figures 3 and 4 show SEM images of corrosion product films and biofilms on the deposit-covered specimens with different thicknesses in abiotic and biotic conditions after 14 d of testing. Meanwhile, the quantitative EDS data are shown in Table S1 in Supplementary Materials (SM). A large number of corrosion products are distributed on the surface of the abiotic bare specimen forming a compact film (Fig. 3(a)).

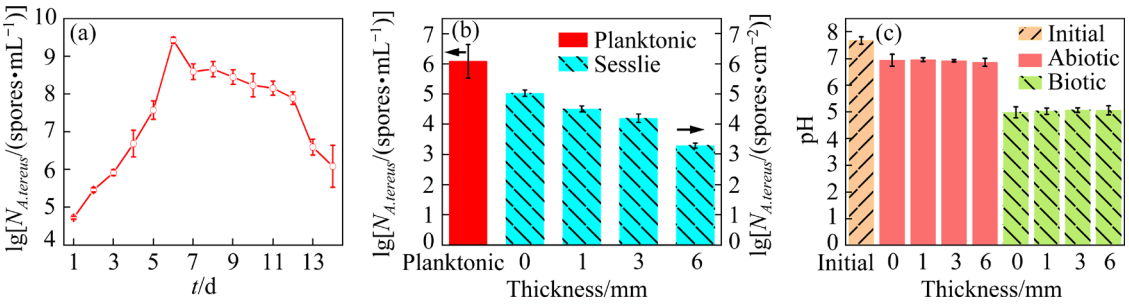

Fig. 2 Growth curve of planktonic *A. terreus* in artificial seawater (a), sessile spores of *A. terreus* after 14 d of testing (b), pH values of test solution in the absence and presence of *A. terreus* initial and after 14 d of testing (c)

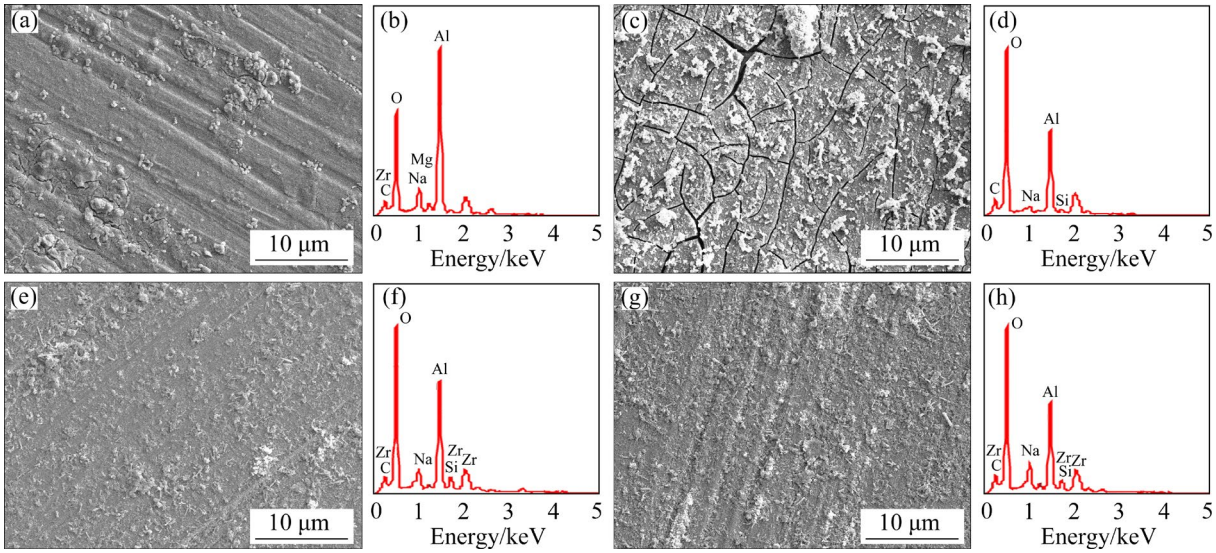

Fig. 3 SEM images (a, c, e, g) and EDS analysis results (b, d, f, h) of corrosion product films on deposit-covered specimens with different thicknesses after 14 d of testing in the absence of *A. terreus*: (a, b) 0 mm; (c, d) 1 mm; (e, f) 3 mm; (g, h) 6 mm

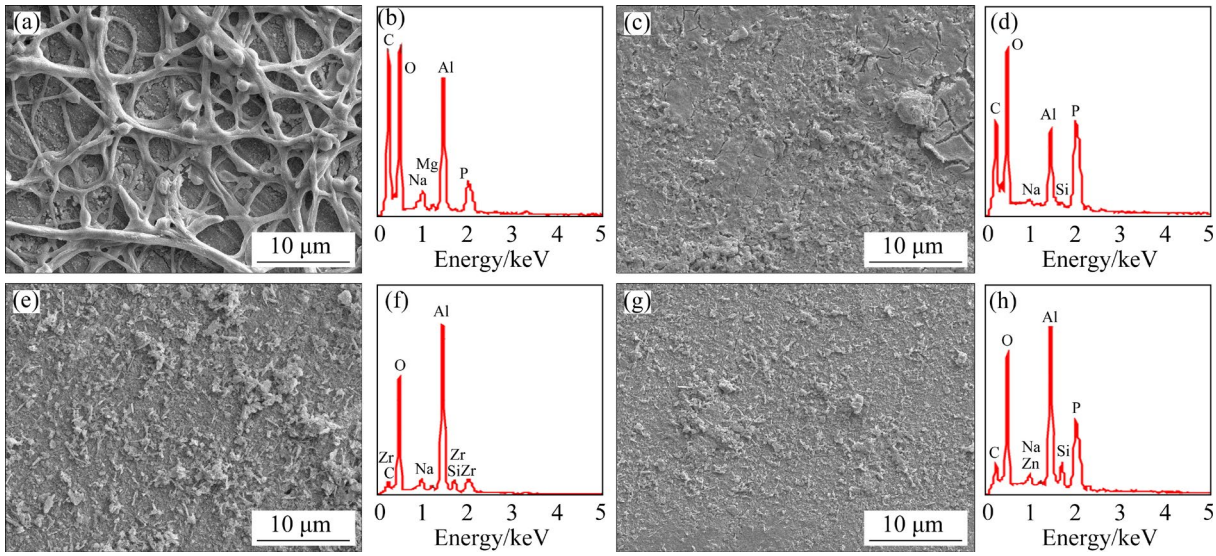

Fig. 4 SEM images (a, c, e, g) and EDS analysis results (b, d, f, h) of corrosion product films and biofilms on deposit-covered specimens with different thicknesses after 14 d of testing in the presence of *A. terreus*: (a, b) 0 mm; (c, d) 1 mm; (e, f) 3 mm; (g, h) 6 mm

Some bulges, cracks, and micropores can be observed in Fig. 3(a). For 1 mm deposit-covered specimen, some amounts of corrosion products can also be observed (Fig. 3(c)). As the thickness of deposits increases from 3 to 6 mm, the scratch line can also be seen even though few corrosion products cover on specimens (Figs. 3(e) and (g)). The decrease of surface corrosion products suggests a slight corrosion in the abiotic environment. The EDS analysis results demonstrate that the dominant elements in corrosion products are O, Al, and C, suggesting the formation of Al_2O_3 or $Al(OH)_3$. Compared to the abiotic conditions, the morphologies of surface films in the presence of *A. terreus* show considerable variation. For the bare specimen, large amounts of hyphae and spores cover the specimen surface (Fig. 4(a)), and high contents of elements C and P can be found correspondingly (Table S1 in SM). Therefore, *A. terreus* can attach and grow well on the surface of bare AA, forming a biofilm. When the deposits with different thicknesses cover specimens, compact films as well as some loose corrosion products are formed (Figs. 4(c−h)). For the 6 mm deposit-covered specimen, the surface film has some cracks (Fig. 4(g)). From EDS analysis results, it is seen that the contents of element C in the surface film have a considerable decrease with the increase of deposit thickness, but the contents of element Al correspondingly increase on the whole (Table S1 in SM). The decrease of C contents in the surface film suggests that the organics in the surface film decline due to the decrease of fungal biological activity caused by deposits. The increase of Al content can derive from the surface Al passive film, also suggesting that the corrosion can be inhibited by the deposits. Combined with the surface morphologies, it can be speculated that *A. terreus* cannot grow well beneath the deposits, potentially due to the presence of anoxic environment. As a result, the actual influence of *A. terreus* on AA7075 corrosion exhibits a noticeable reduction with the increase in deposit thickness. Consequently, the chemical compositions of the surface films on 6 mm deposit-covered abiotic and biotic specimens turn out to be similar.

3.3 XRD analysis results

Figure 5 presents XRD analysis results of surface corrosion products on specimens covered with different deposit thicknesses in the absence and presence of *A. terreus*. In the abiotic and biotic test environments, the species of corrosion products are similar, i.e., $Al(OH)_3$ and Al_2O_3, which are consistent with EDS data (Table S1 in SM). The peaks derived from corrosion products are weak because the corrosion type of AA7075 is localized corrosion, not uniform corrosion due to the rapidly formed passive film. The presence of $Al(OH)_3$ suggests the part damage of AA passive film. Furthermore, AA passive film is easily destroyed in biotic conditions [27].

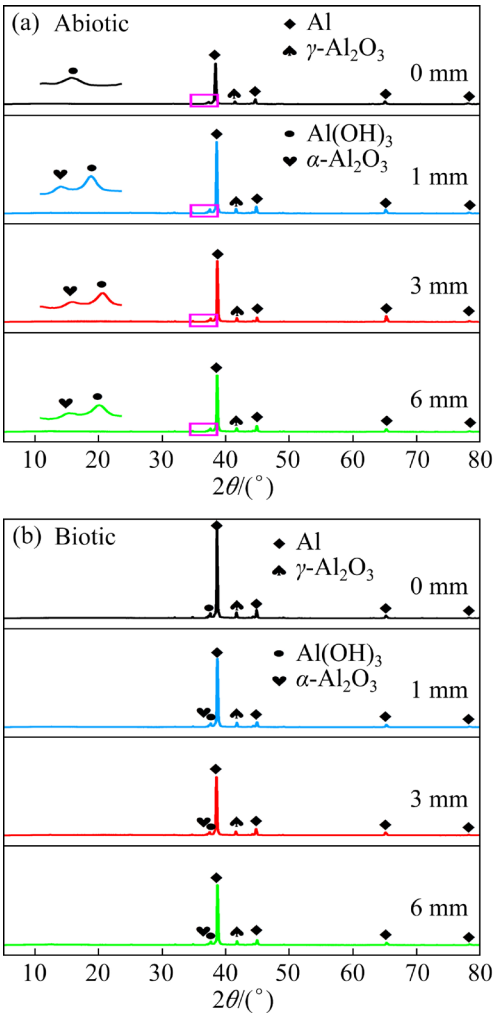

Fig. 5 XRD patterns of corrosion products on deposit-covered specimens with different thicknesses after 14 d of testing in the absence (a) and presence (b) of *A. terreus*

3.4 Bare surface morphologies caused by corrosion

The bare surface morphologies of deposit-covered specimens caused by corrosion after 14 d of testing in the abiotic and biotic conditions are presented in Fig. 6. In the absence of *A. terreus*, a

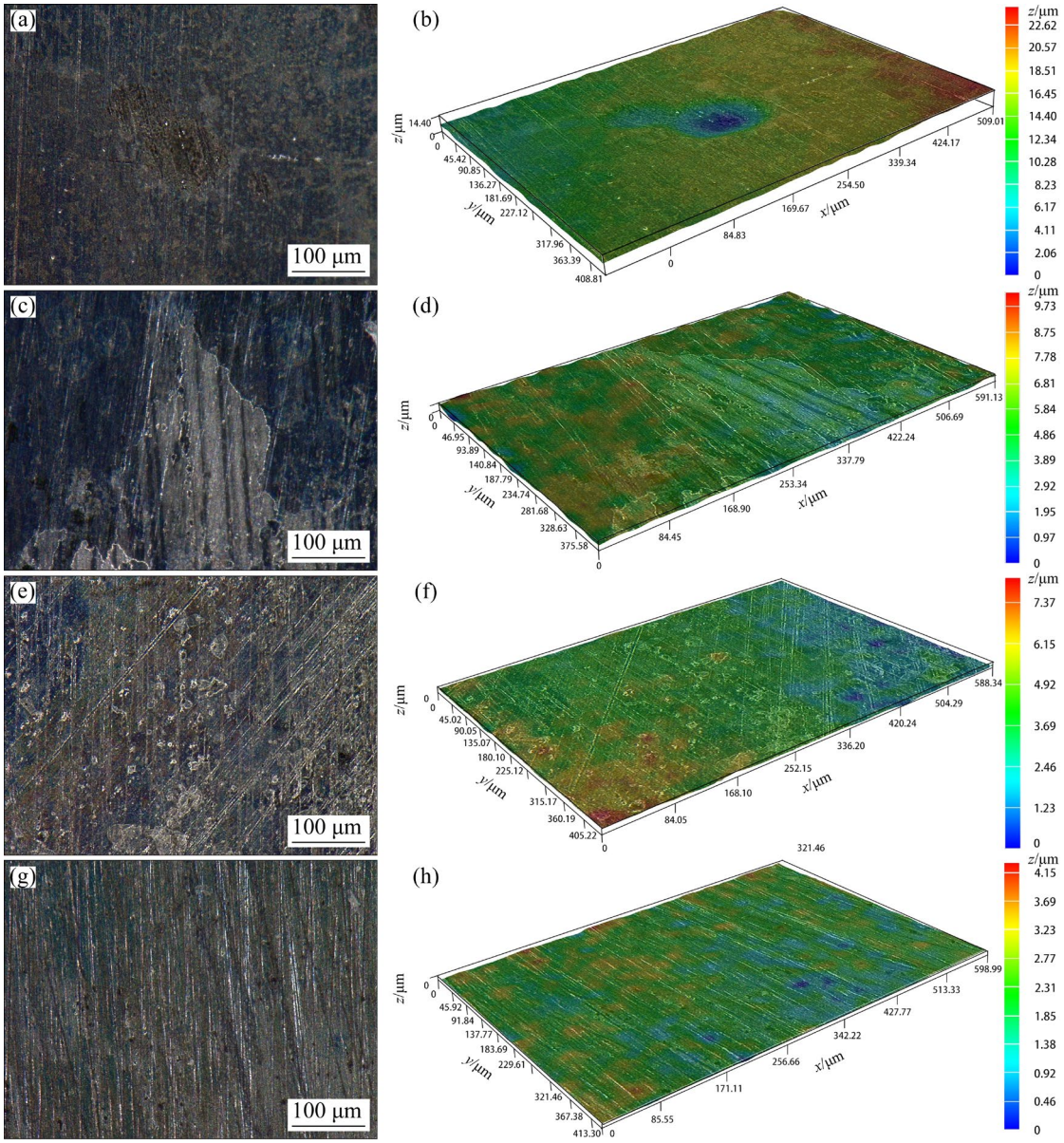

Fig. 6 3D bare surface morphologies of deposit-covered specimens with different thicknesses caused by corrosion after 14 d of testing in the absence of *A. terreus*: (a, b) 0 mm; (c, d) 1 mm; (e, f) 3 mm; (g, h) 6 mm

small corrosion pit with a depth of about 22.62 μm can be observed for the bare specimen, and the polish lines can also be identified, suggesting a slight corrosion (Figs. 6(a, b)). Some tiny corrosion pits are shown on specimens as the deposit thickness increases, but the changes are inconspicuous (Figs. 6(c, d)). Therefore, the presence of a deposit on the specimen has an inhibition effect on AA corrosion. In a conclusion, the abiotic corrosion of the bare and deposit-covered specimens is not severe. However, the corrosion can be considerably enhanced by *A. terreus* compared with abiotic conditions. For the bare specimen, much more serious pitting corrosion induced by *A. terreus* is presented in Figs. 7(a, b). Similarly, pitting corrosion is also found for the deposit-covered specimens of 1, 3, and 6 mm, but the pitting corrosion is slight (Figs. 7(c−h)). Therefore, AA corrosion induced by *A. terreus* is also inhibited by deposits.

3.5 Open circuit potential analysis results

Time-dependent OCP vales of the control and biotic deposit-covered specimens with different thicknesses are monitored, which are shown in Fig. 8. In the abiotic conditions, the deposits of 1 and 3 mm promote the negative shift of OCP, while deposit of 6 mm causes a positive shift compared

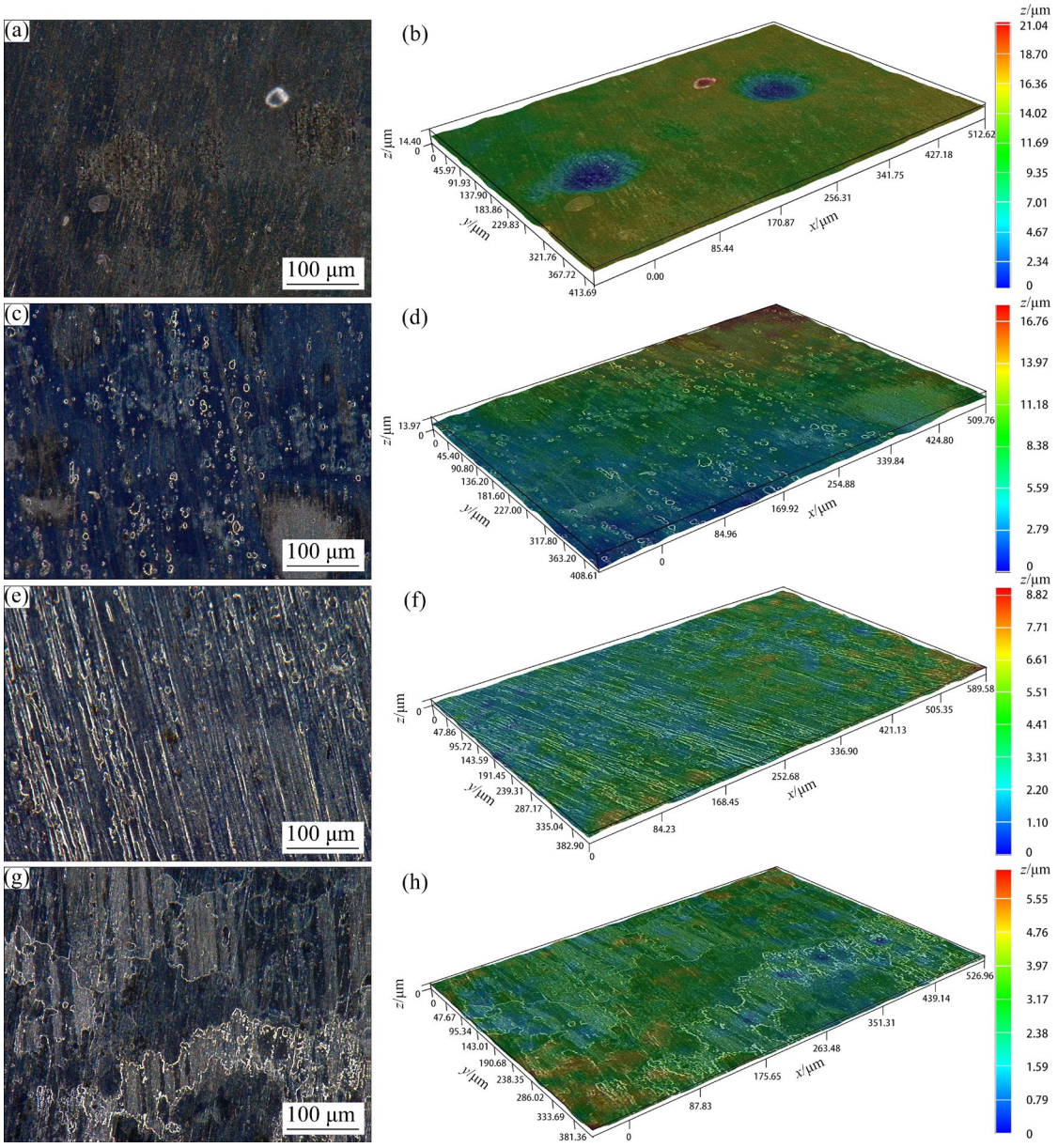

Fig. 7 3D bare surface morphologies of deposit-covered specimens with different thicknesses caused by corrosion after 14 d of testing in the presence of *A. terreus*: (a, b) 0 mm; (c, d) 1 mm; (e, f) 3 mm; (g, h) 6 mm

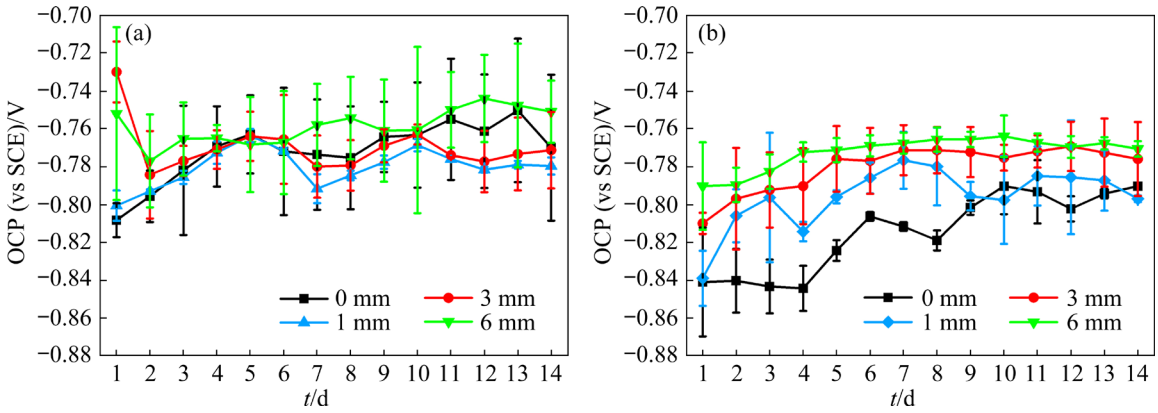

Fig. 8 Changes of OCP of bare and deposit-covered specimens with time in artificial seawater in the absence (a) and presence (b) of *A. terreus*

with the bare specimen (Fig. 8(a)). It is obvious that the OCP values in the abiotic control conditions are higher than these in the presence of *A. terreu*, i.e., *A. terreus* can promote the shift of OCP in a negative direction (Figs. 8(a, b)). Furthermore, the OCP values of the deposit-covered specimens are much more positive compared with the bare specimen, and there is an OCP difference for specimens beneath the deposits and the bare specimens (Fig. 8(b)).

3.6 EIS data

Figures 9, 10 and S1, S2 (in SM) show the effects of deposit thickness and test time on Nyquist and Bode plots of specimens in the abiotic and biotic environments. For the abiotic control conditions, the impedances of bare specimen decline steadily during the initial 10 d due to the diameter compression of Nyquist plots, which can derive from the slow damage of the passive film caused by Cl^- (Fig. 9(a)) [28−31]. However, the visible increase of semi-circle in the following days can be observed (Fig. 9(a)). Compared with bare specimen, the Nyquist plots of deposit-covered specimens have larger diameters, suggesting a higher impedance. Furthermore, the broad phase angles of deposit-covered specimens suggest that the surface passive film of specimens is good due to the influence of deposits, thus leading to a higher impedance. In addition, AA7075 corrosion is affected by the deposit thickness, and the thicker the deposit, the lower the corrosion rate.

In the biotic artificial seawater, the impedance values of the bare specimen decrease apparently from the Nyquist plots during initial 7 d, suggesting that *A. terreus* can destroy AA7075 passive film (Fig. 10(a)). Then, the diameters of Nyquist plots gradually increase with the increase of time (Fig. 10(a)). There is an additional phase angle formed in the low-frequency region (Fig. S2(b) in SM) demonstrating the formation of a biofilm on specimen shown in Fig. 4(a). The variations of Nyquist plots of 1 mm deposit-covered specimen are close to those of the bare specimen but with higher impedance values (Figs. 10(a, b)). For the specimens with deposit thicknesses of 3 and 6 mm, the diameters of Nyquist plots decrease continuously in the first 10 d and then increase

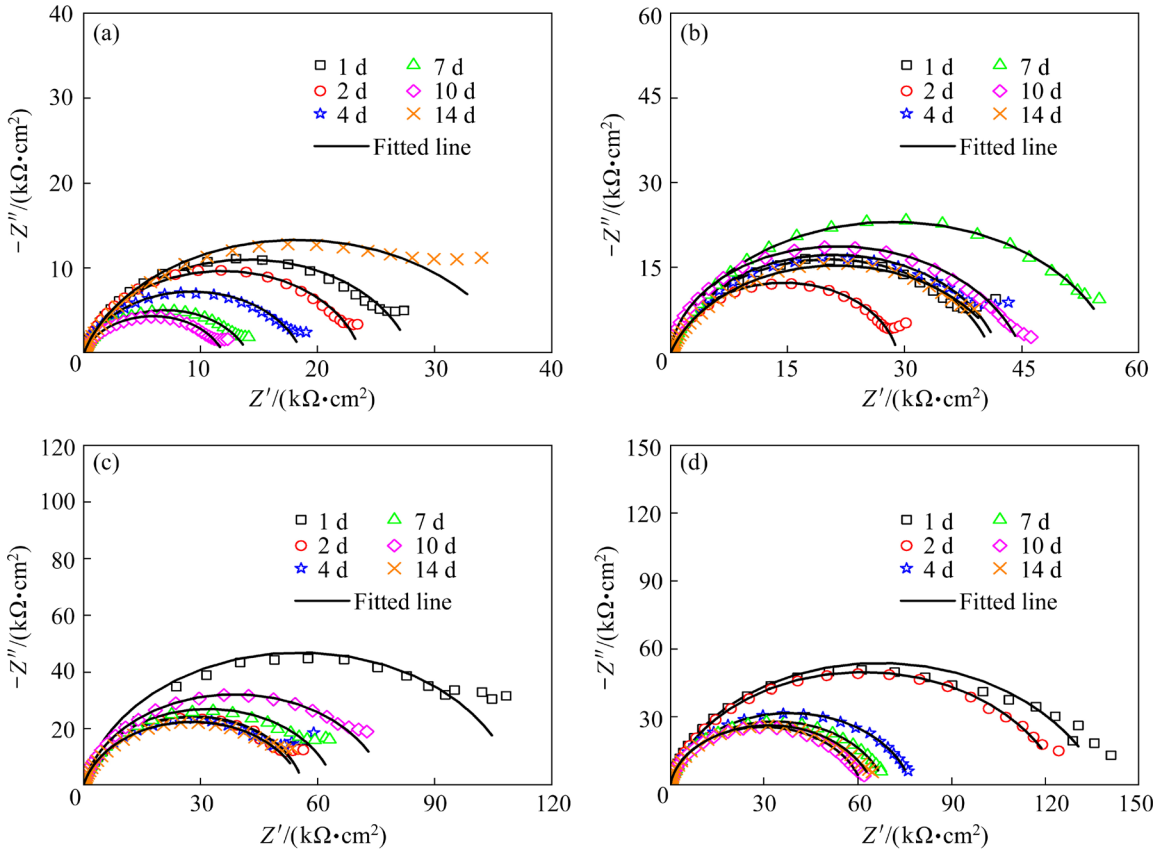

Fig. 9 Effects of deposit thickness and test time on Nyquist plots of abiotic specimens: (a) 0 mm; (b) 1 mm; (c) 3 mm; (d) 6 mm

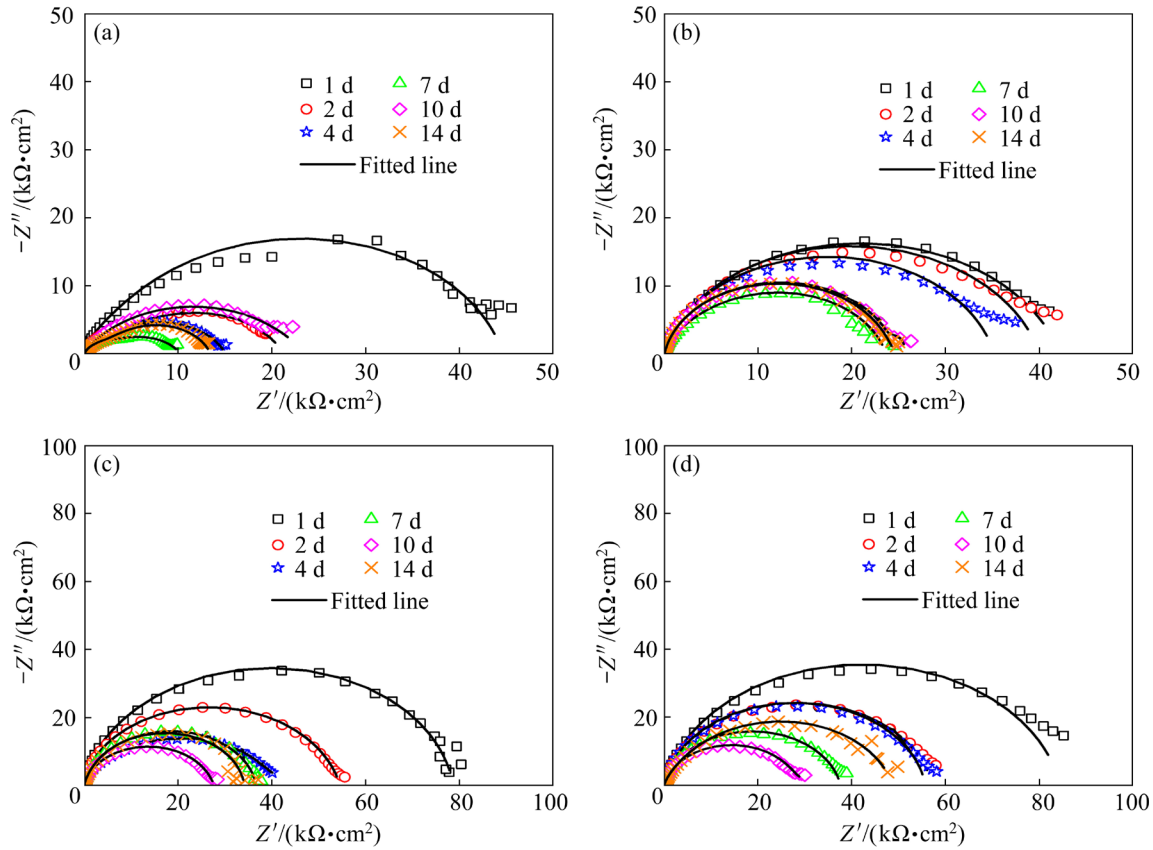

Fig. 10 Effects of deposit thickness and test time on Nyquist plots of specimens with *A. terreus*: (a) 0 mm; (b) 1 mm; (c) 3 mm; (d) 6 mm

slightly (Figs. 10(c, d)). The broad phase angles of the 3 and 6 mm deposit-covered specimens are consistent with those of the abiotic control conditions, demonstrating that even though *A. terreus* can accelerate AA7075 corrosion, their influence on corrosion turns out to be small for the thicker deposit.

An equivalent circuit including two time-constants (Fig. S3 in SM) is used to fit the above EIS data, and the fitted results are presented in Fig. 11. In the equivalent circuit, R_s, R_f, and R_{ct} are assigned to the solution resistance, surface film resistance, and charge transfer resistance, respectively, while Q_f and Q_{dl} correspond to film capacitance and double layer capacitance, respectively. A constant phase angle element (CPE) is used considering the heterogeneous surface films caused by corrosion, and it reflects the natural corrosion process that deviates from the ideal capacitance [32]. The fitted parameter of EIS, i.e., R_p, is the sum of R_f and R_{ct}. There is a significant increase in R_p values as the deposit reaches 6 mm compared with the bare specimen whether in the presence of *A. terreus* or not (Figs. 11(a, b)). The R_p values of the biotic specimens in the presence of *A. terreus* are lower than those in abiotic conditions. Therefore, fungus *A. terreus* can considerably improve the corrosion rate of AA7075 but the deposits effectively inhibit AA7075 corrosion. Furthermore, the change trends of R_p values have a large difference in the abiotic and biotic environments (Figs. 11(a, b)), and *A. terreus* can cause a fast decrease of R_p values during the initial several days (Fig. 11(b)) but the presence of deposits can decline the corrosion acceleration effect induced by *A. terreus*.

3.7 Potentiodynamic polarization curves

The measured potentiodynamic polarization curves of deposit-covered specimens on the 14th day in abiotic and biotic environments are presented in Fig. 12. The anodic dissolution of Al and the cathodic oxygen reduction reactions are inhibited by deposits in the abiotic control conditions (Fig. 12(a)). The increase of deposit thickness can cause a small corrosion current density. The

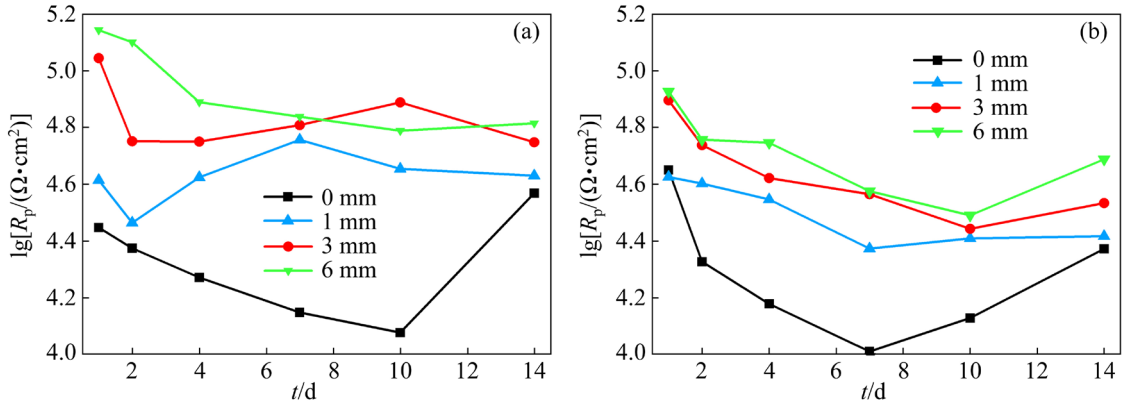

Fig. 11 Changes of R_p, i.e., R_f+ R_{ct}, fitted from EIS data with time for specimens in the absence (a) and presence (b) of *A. terreus*

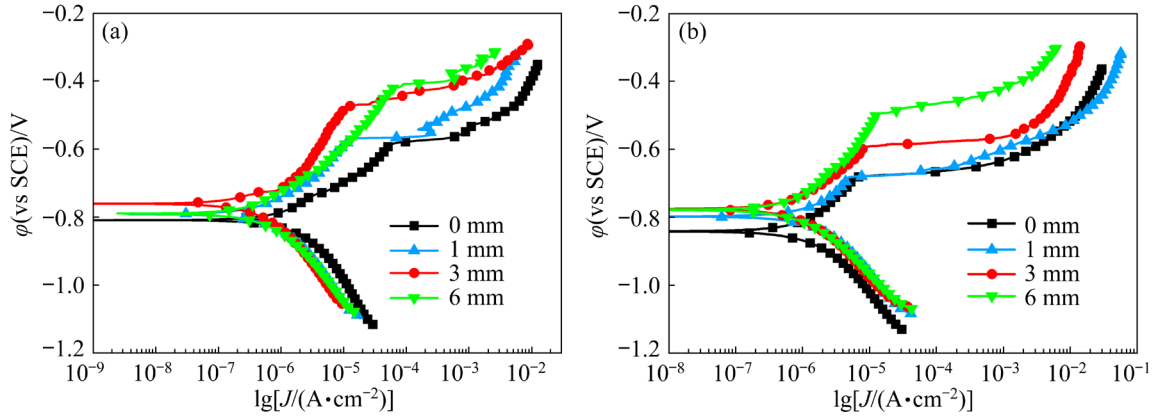

Fig. 12 Potentiodynamic polarization curves of specimens after 14 d of testing in the absence (a) and presence (b) of *A. terreus*

presence of the deposit possibly inhibits the diffusion of dissolved oxygen to the water–electrode interface, thus causing a decrease in the cathodic oxygen reduction reaction rate. In the biotic seawater containing *A. terreus*, deposits mainly inhibit the anodic dissolution of Al, but the cathodic reaction changes little with the increase of deposit thickness (Fig. 12(b)). Furthermore, it is also observed that *A. terreus* promotes the positive shift of the corrosion current density compared to the control, i.e., *A. terreus* improves AA corrosion rate. The fitted parameters of the polarization curves are presented in Table S2 in SM. It is seen from Table S2 in SM that the corrosion current densities of specimens decrease with the increase of deposit thickness whether in the biotic or abiotic conditions. Furthermore, the corrosion current densities of specimens in the presence of *A. terreus* are higher than those under the abiotic control, suggesting the corrosion acceleration caused by *A. terreus* (Table S2 in SM).

3.8 Galvanic current density distribution of WBE

The deposit of 3 mm is used to study the localized corrosion behavior of the specimen beneath the deposits induced by *A. terreus* based on WEB. Figures 13 and 14 show the changes in abiotic and biotic galvanic current density distributions of 3 mm deposit-covered specimens with time. For the abiotic control WBE, some small anodes can be easily found, and some of these anodes can change their position with time suggesting that the formation of localized corrosion is a dynamic process (Fig. 13). The appearance of the small anodes also corresponds to the pitting corrosion shown in Figs. 6(e, f). The anodic current density of the single peak increases with the increase of time, and it reaches a maximum value on the 7th day, i.e., 9.3×10^{-7} A/cm^2, then it turns out to be smaller. The small current density of these anodic sites demonstrates slight pitting corrosion (Figs. 6(e, f)). In the biotic artificial seawater

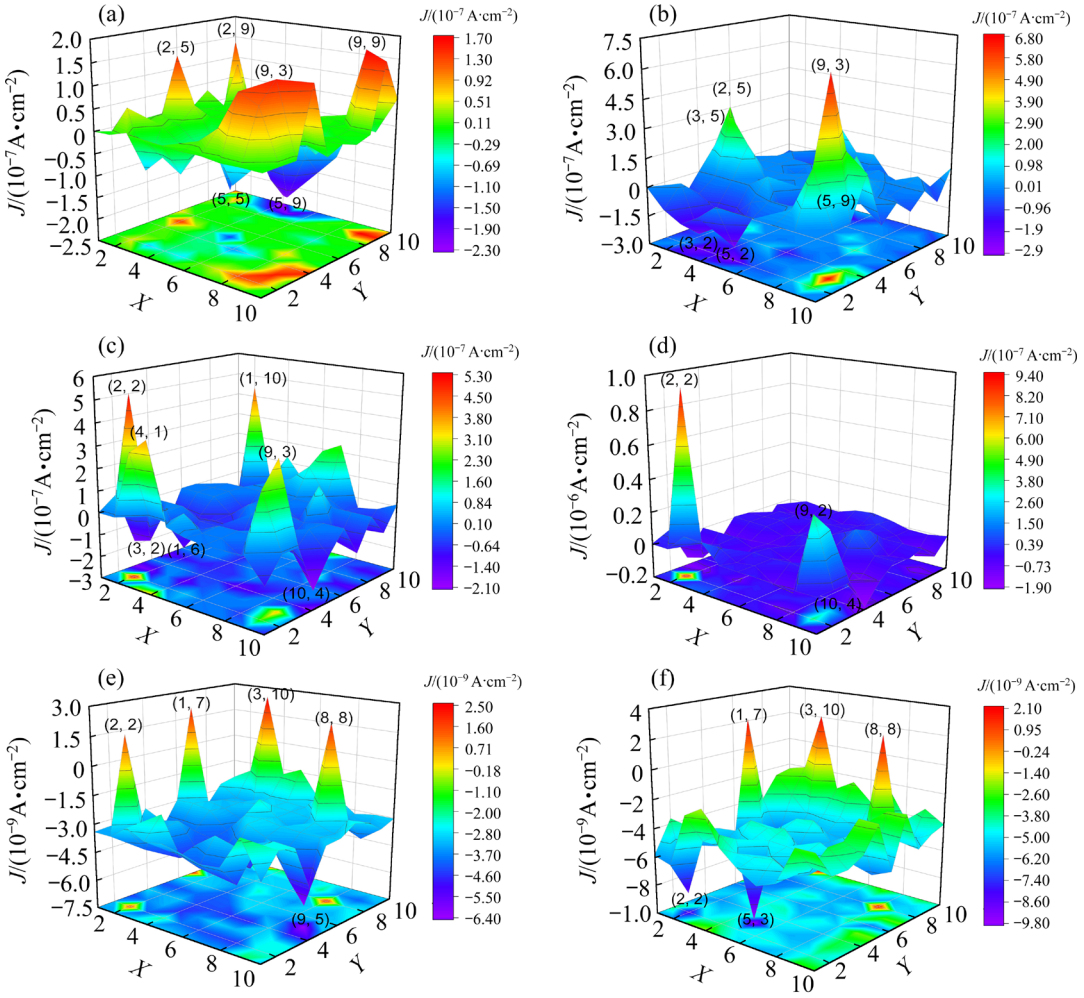

Fig. 13 Galvanic current density distributions of 3 mm deposit-covered abiotic control specimen with time in artificial seawater: (a) 1 d; (b) 2 d; (c) 4 d; (d) 7 d; (e) 10 d; (f) 14 d (*X*: Horizontal position of electrodes; *Y*: Vertical position of electrodes)

containing *A. terreus*, some small anodes are also observed, but these anodes can be quickly formed (Fig. 14). The maximum peak value of anodic current density is 4.3×10^{-6} A/cm^2 obtained also on the 7th day (Fig. 14(d)), which is considerably higher than the abiotic control condition. The anodic peak current density turns out to be smaller after 7 d of testing. Therefore, the localized corrosion should be slight, which is consistent with the bare corrosion morphologies (Figs. 7(e, f)). However, the WBE analysis results further demonstrate that *A. terreus* has enhanced the localized corrosion of the specimens beneath the deposits.

3.9 Galvanic current density between bare and deposited specimens

The driving force of galvanic corrosion can be determined by the values of OCP difference. Generally, a higher potential difference value can accelerate the galvanic effects [33]. The time-dependent OCP differences between the specimens covered with and without 3 mm deposit in abiotic and biotic environments are presented in Fig. S4 in SM. In the abiotic conditions, the difference values of OCP decrease with the increase of time, and the galvanic effect is very low due to the small difference values of OCP from the 4th to the 10th day. The initially positive OCP difference values and the latterly negative OCP difference values demonstrate the polarity inversion in galvanic coupling. However, the difference values of OCP induced by *A. terreus* are larger than those in abiotic conditions.

Figure 15 shows the time-dependent abiotic and biotic galvanic current density between the bare

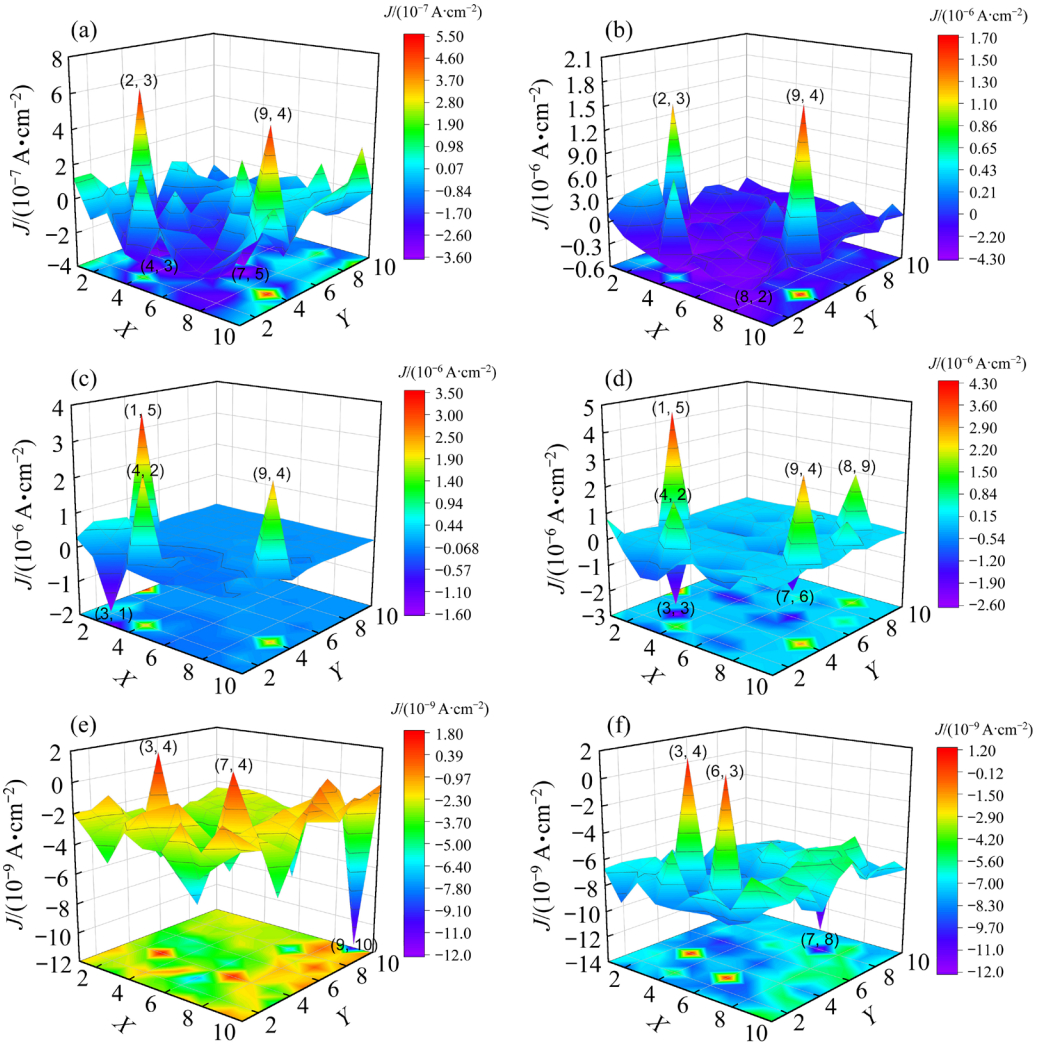

Fig. 14 Galvanic current density distributions of 3 mm deposit-covered specimen with time in artificial seawater containing *A. terreus*: (a) 1 d; (b) 2 d; (c) 4 d; (d) 7 d; (e) 10 d; (f) 14 d

and 3 mm deposit-covered specimens in artificial seawater. In the abiotic conditions, the bare specimen is anode while the deposit-covered specimen is cathode during initial 4 d, and the polarity inversion is formed after 7 d of testing due to the appearance of negative galvanic current density. In the biotic environment, the anode is the bare specimen while the cathode corresponds to the deposit-covered specimen. However, the values of galvanic current density are not large both in the abiotic and biotic environments. These indicate that the galvanic corrosion effect of the specimens covered with and without deposits is weak, which is different from the previous reports of UDC for steel [20,34,35]. But *A. terreus* can still accelerate the galvanic corrosion of the bare and deposit-covered specimens. Hence, the species of microorganism and alloy types both can influence the galvanic corrosion behavior derived from the deposits.

4 Discussion

4.1 Abiotic corrosion of deposit-covered AA7075

Aluminum alloys usually have a high corrosion resistance due to the surface passive film, but they can also suffer serious localized corrosion, especially in marine environments [36,37]. This work also confirms the serious pitting corrosion of AA7075 in artificial seawater (Figs. 6(a, b)). The pitting corrosion is probably caused by Cl^- due to the part damage of the passive film. However, the corrosion behavior and mechanism have changed for the deposit-covered specimens compared with

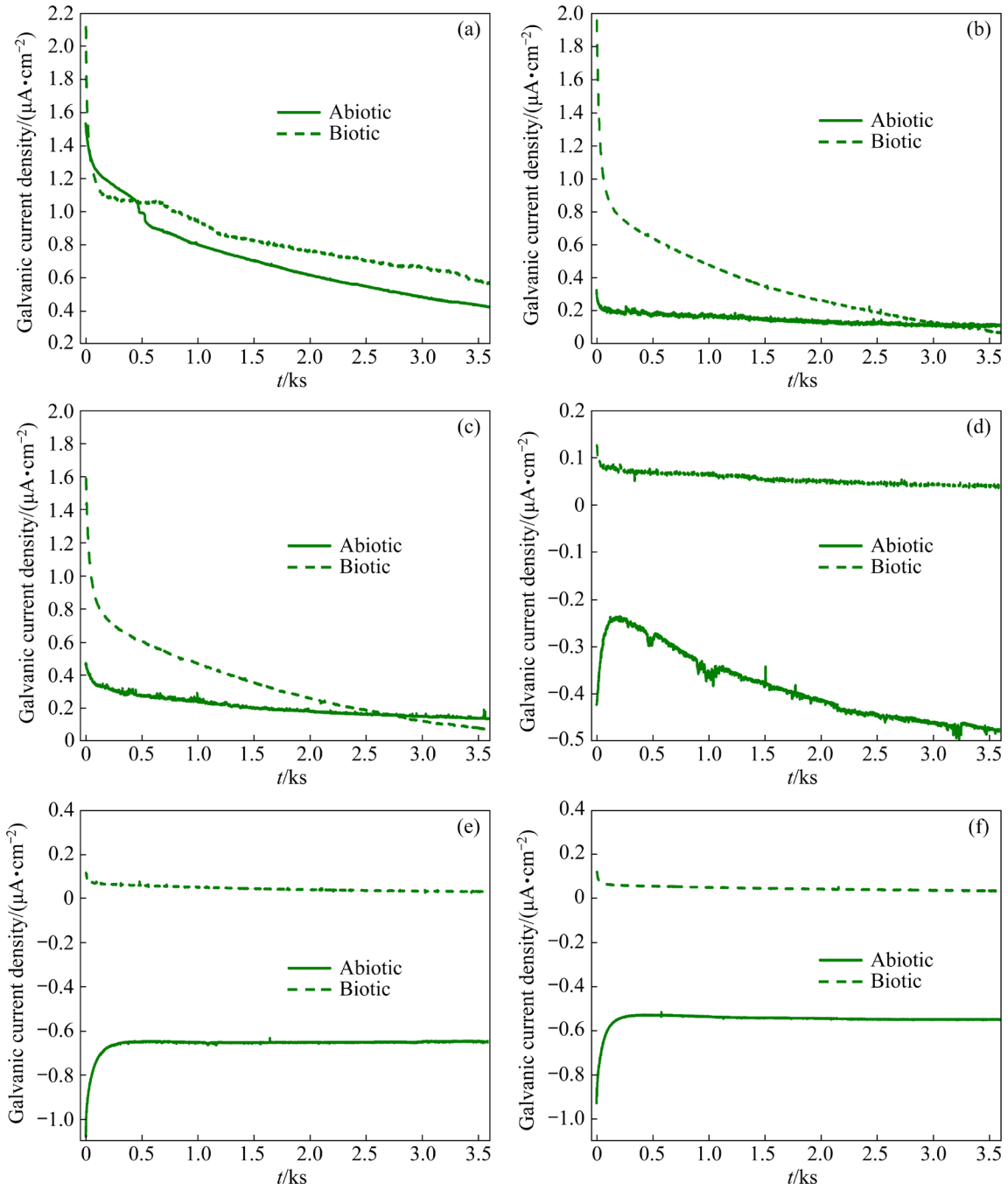

Fig. 15 Changes of galvanic current density between bare and 3 mm deposit-covered specimens with time in abiotic and biotic artificial seawater: (a) 1 d; (b) 2 d; (c) 4 d; (d) 7 d; (e) 10 d; (f) 14 d

the bare specimens. Some previous studies [26,38−40] found that the existence of deposits can enhance the localized corrosion of carbon steel, which is contrary to the experimental results in this study. According to the experimental results, the covered deposits can inhibit both uniform and pitting corrosion (Figs. 6, 11 and 12). Furthermore, the thicker deposits have a higher inhibition effect against AA7075 corrosion (Fig. 11). A difference between AA7075 and carbon steel is the passive film. The existence of the passive film will cause a change in the corrosion beneath the deposits.

The covered deposits on AA7075 have a blocking effect on dissolved oxygen diffusion and dissolved metal cations [24], i.e., the deposits can effectively inhibit both the anodic and cathodic reactions resulting in corrosion inhibition compared to the bare AA7075. Because of the appearance of a

passive film, AA7075 only can initiate corrosion on the local weak area of the passive film with the assistance of Cl^- [41]. Therefore, the total dissolution rate of Al should be very slow. Furthermore, the electron from the dissolution of Al cannot be easily transferred to the cathodic oxygen because of the poor electrical conductivity of AA7075 passive film. Therefore, the formation of a galvanic corrosion cell for AA7075 beneath the deposits is difficult and its efficiency should be low not like the situation of deposit-covered steel. As a result, the pitting corrosion and uniform corrosion of deposit-covered AA7075 are inhibited by the deposits, and the thicker deposits have a higher corrosion inhibition effect on AA7075 corrosion. Even if the corrosion of deposit-covered AA7075 mitigates, pitting corrosion can also be found due to the penetration of Cl^- and the existence of small amounts of O_2 beneath depositions. Therefore, a slight pitting corrosion for the deposit-covered specimens is observed from the bare surface morphologies (Figs. 6 and 7). WBE results also confirm the slight pitting corrosion due to the formation of the small anode peaks with a weak current density.

A weak galvanic corrosion effect of the AA7075 specimens with and without deposits is also found (Fig. S4 in SM and Fig. 15), which is also different from the situations formed by the bare and deposit-covered carbon steel. Moreover, the galvanic current density (J_g) is calculated according to the following equation [42]:

$$\ln J_g = \frac{\beta_{c2}}{\beta_{a1}+\beta_{c2}} \ln(A_2 J_{corr2}) + \frac{\beta_{a1}}{\beta_{a1}+\beta_{c2}} \ln(A_1 J_{corr1}) + \frac{\varphi_{corr2} - \varphi_{corr1}}{\beta_{a1} + \beta_{c2}} \quad (1)$$

where φ_{corr1} and φ_{corr2} are the corrosion potentials of Electrodes 1 and 2, respectively; J_{corr1} and J_{corr2} are the corrosion current densities of Electrodes 1 and 2, respectively; β_{a1}, β_{a2}, and β_{c1}, β_{c2} are Tafel slopes of the anodic and cathodic reactions for Electrodes 1 and 2, respectively.

The galvanic effect is determined by the differences between φ_{corr2} and φ_{corr1} according to Eq. (1). The small potential differences shown in Fig. 14 in the abiotic conditions demonstrate a weak galvanic effect. Furthermore, the polarity inversion is found, which is probably caused by the corrosion product film formed on AA7075 [43]. This corrosion product film promotes the positive shift of OCP of the bare AA7075.

4.2 Corrosion acceleration of deposit-covered AA7075 induced by *A. terreus*

A. terreus can survive well and maintain good biological activity in artificial seawater so that a biofilm is easily formed on AA7075 (Figs. 2 and 3). *A. terreus* possesses high corrosivity for AA, and it can easily cause pitting corrosion [17,27,44]. Severe pitting corrosion of bare AA7075 resulting from *A. terreus* is also observed in this work (Figs. 7(a, b)). Fungi can directly or indirectly accelerate AA7075 corrosion. The direct way is related to the electron transfer directly from Al to fungi through some electronic conductors, such as hyphae. Because some fungi can directly use some elements, including Fe, Zn, Cu, and Mg, from AA as their nutrients to increase their metabolic activity [45]. Furthermore, fungi can secret large amounts of extracellular polymeric substances (EPS) which are composed of proteins, polysaccharides, and organic acids. The proteases and organic acids have been verified to effectively increase corrosion rate of AA [44,46,47]. The pH values in the presence of *A. terreus* also have a considerable decrease after 14 d of testing (Fig. 2(c)), suggesting a biogenic acid corrosion. Therefore, the corrosion acceleration of the bare AA7075 is easily induced by *A. terreus*.

However, the corrosion behavior of deposit-covered AA7075 caused by *A. terreus* will have a high difference in comparison with the bare specimens. Initially, *A. terreus* cannot survive well beneath the deposits, and the count of sessile spores has a fast decrease with the increase in deposit thickness (Fig. 2(b)). The decrease of sessile spores beneath the deposits is due to two respect reasons. Initially, as discussed above, the existence of a deposit can inhibit the diffusion of oxygen. The anoxic environment is detrimental to the growth of aerobic *A. terreus*. Secondly, *A. terreus* beneath deposits cannot get the organic nutrients easily. The sessile microorganisms are mainly responsible for MIC [48]. This means that the direct corrosion acceleration of *A. terreus* for AA7075 is gradually weakened with the increase of deposit thickness, but the indirect actions of *A. terreus* such as organic acids and extracellular proteases, can also

accelerate the corrosion of deposit-covered AA7075. WBE analysis results indicate that *A. terreus* accelerates the localized corrosion due to the formation of some anodic peaks with a higher current density than those in abiotic conditions (Figs. 13 and 14). Therefore, *A. terreus* can promote under-deposit corrosion, but the corrosion acceleration effect of *A. terreus* will be weakened with the increase in deposit thickness.

It is also found that *A. terreus* can accelerate the galvanic corrosion between the specimen beneath a 3 mm deposit and the bare specimen (Fig. 9, Fig. S1 in SM and Fig. 15). As stated in Eq. (1), the galvanic effect is determined by the potential difference. *A. terreus* can deeply affect the bare AA7075 corrosion and cause a negative shift of OCP (Fig. 8). Thus, a large potential difference between φ_{corr1} and φ_{corr2} in the presence of *A. terreus* is formed, leading to the enhancement of galvanic effect of the bare and deposit-covered AA7075. However, the biological activity of *A. terreus* shows a fast decrease during the later period which can cause the decrease of galvanic effect [35]. Therefore, the galvanic current density decreases gradually as time goes on so that the values of anodic galvanic current density tend to be small during the last 4 d (Fig. 15). As discussed above, the galvanic effect for AA7075 is small whether in abiotic and biotic conditions not like carbon steel. The pitting corrosion mechanisms of the AA7075 under the bare and deposit-covered conditions in the absence and presence of *A. terreus* are proposed and presented in Fig. 16. The formation of AA passive film and the presence of *A. terreus* both can affect under-deposit corrosion [49].

5 Conclusions

(1) In abiotic conditions, a thin corrosion product film is formed on AA7075, meanwhile, the polish line can be recognized. Pitting corrosion of the abiotic bare AA7075 with a depth of 22.62 μm can be found. With the increase in deposit thickness, both the pitting corrosion and uniform corrosion are alleviated. Beneath the deposits, some small anodic sites are found but with a small current density from WBE results, suggesting a slight pitting corrosion. There is weak galvanic corrosion derived from the bare and 3 mm deposit-covered AA7075.

(2) In the biotic conditions, *A. terreus* survives well and can maintain good biological activity, but the sessile *A. terreus* declines apparently with the increase of deposit thickness. For the bare AA7075, there are large amounts of hyphae and spores, but no recognized hyphae and spores can be found beneath the deposits.

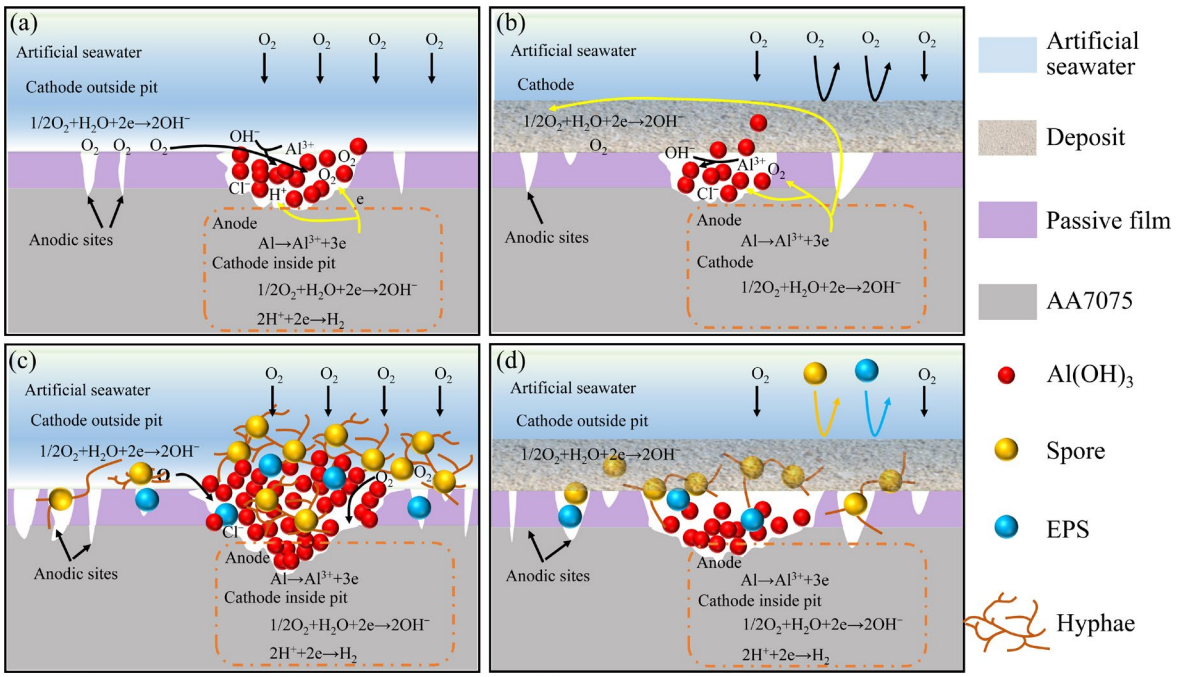

Fig. 16 Schematic diagrams of pitting corrosion mechanism of bare and deposit-covered specimens in the absence (a, b) and presence (c, d) of *A. terreus* in artificial seawater

(3) Compared to abiotic control, *A. terreus* apparently enhances the corrosion of AA7075. The corrosion of AA7075 caused by *A. terreus* is also inhibited by deposits. There is a good passive film for the specimens covered with a thicker deposit. The formation of small anodes and large cathodes contributes to the pitting corrosion beneath the deposits. *A. terreus* not only accelerates under-deposit corrosion but also enhances the galvanic corrosion induced by deposits.

CRediT authorship contribution statement

Jia-ping WANG: Conceptualization, Data curation, Investigation, Formal analysis, Writing − Original draft; **Yi ZHANG:** Visualization, Methodology; **Hong-wei LIU:** Conceptualization, Formal analysis, Writing − Review & editing, Supervision, Funding acquisition; **Yan-sheng YIN:** Conceptualization, Methodology, Supervision.

Declaration of competing interest

The authors declare that they have no known competing financial interests or personal relationships that could have appeared to influence the work reported in this paper.

Acknowledgments

This research was supported by Guangdong Basic and Applied Basic Research Foundation, China (No. 2023A1515012146), and the National Natural Science Foundation of China (No. 52271083).

Supplementary Materials

Supplementary Materials in this paper can be found at: http://tnmsc.csu.edu.cn/download/03-p1406-2023-0989-Supplementary_Materials.pdf.

References

[1] GUO Fu-qiang, DUAN Shu-wei, WU Dong-ting, MATSUDA K, WANG Tao, ZOU Yong. Facile etching fabrication of superhydrophobic 7055 aluminum alloy surface towards chloride environment anticorrosion [J]. Corrosion Science, 2021, 182: 109262.

[2] SOKOLUK M, CAO Che-zheng, PAN Shuai-hang, LI Xiao-chun. Nanoparticle-enabled phase control for arc welding of unweldable aluminum alloy 7075 [J]. Nature Communications, 2019, 10(1): 98.

[3] ZHAO Ning, SUN Qian, PANG Qiu, HU Zhi-li. Comprehensive study of hot compression behaviors and microstructure evolution of solutionized 6082 aluminum alloy extruded bar [J]. Journal of Alloys and Compounds, 2023, 931: 167541.

[4] ZHAO Ning, MA Hui-juan, SUN Qian, HU Zhi-li, YAN Yang, CHEN Tian-fu, HUA Lin. Microstructural evolutions and mechanical properties of 6082 aluminum alloy part produced by a solution-forging integrated process [J]. Journal of Materials Processing Technology, 2022, 308: 117715.

[5] INGLE A, HEURTAULT S, HAFID F, SAID J, PROIETTI A, ODEMER G, DEHMAS M, BLANC C. Identification of the critical microstructural parameters on the corrosion behaviour of commercially pure aluminium alloy [J]. Corrosion Science, 2022, 208: 110654.

[6] WANG Ming-tao, WANG Li-wei, YANG Wen-di, LIU Yu-xi, TERRYN H, CUI Zhong-yu. Study on the roles of bisulfite in the stress corrosion cracking of 7050-T7451 aluminum alloy in the thin electrolyte layer environment [J]. Corrosion Science, 2023, 215: 111030.

[7] SHEN Yuan-yuan, DONG Yao-hua, ZHU Hong-ling, DONG Li-hua. Pseudomonas xiamenensis in the cutting fluids on corrosion behavior of aluminum alloy 2219 [J]. Bioelectrochemistry, 2023, 150: 108350.

[8] RAJASEKAR A, TING Y P. Microbial corrosion of aluminum 2024 aeronautical alloy by hydrocarbon degrading bacteria *Bacillus cereus* ACE4 and *Serratia marcescens* ACE2 [J]. Industrial & Engineering Chemistry Research, 2010, 49(13): 6054−6061.

[9] LITTLE B J, BLACKWOOD D J, HINKS J, LAURO F M, MARSILI E, OKAMOTO A, RICE S A, WADE S A, FLEMMING H C. Microbially influenced corrosion—Any progress? [J]. Corrosion Science, 2020, 170: 108641.

[10] XU Li-ting, GUAN Fang, MA Yan, ZHANG Rui-yong, ZHANG Yi-meng, ZHAI Xiao-fan, DONG Xu-cheng, WANG Ya-nan, DUAN Ji-zhou, HOU Bao-rong. Inadequate dosing of THPS treatment increases microbially influenced corrosion of pipeline steel by inducing biofilm growth of Desulfovibrio hontreensis SY-21 [J]. Bioelectrochemistry, 2022, 145: 108048.

[11] LIU Feng-ling, ZHANG Jie, SUN Cai-xia, YU Zhen-hua, HOU Bao-rong. The corrosion of two aluminium sacrificial anode alloys in SRB-containing sea mud [J]. Corrosion Science, 2014, 83: 375−381.

[12] ARROUSSI M, ZHAO Jin-long, BAI Chun-guang, ZHANG Shu-yuan, XIA Zhi-zhou, JIA Qing, YANG Ke, YANG Rui. Evaluation of inhibition effect on microbiologically influenced corrosion of Ti−5Cu alloy against marine *Bacillus vietnamensis* biofilm [J]. Bioelectrochemistry, 2023, 149: 108265.

[13] LIU Hong-wei, XU Da-ke, DAO A Q, ZHANG Guo-an, LV Ya-lin, LIU Hong-fang. Study of corrosion behavior and mechanism of carbon steel in the presence of *Chlorella vulgaris* [J]. Corrosion Science, 2015, 101: 84−93.

[14] LIAO Wen-pei, LIU Hai-xian, JIN Zheng-yu, WANG Zhi, LIU Hong-wei. Synergistic inhibition effect of ultraviolet irradiation and benzalkonium chloride on the corrosion of 316L stainless steel caused by *Aspergillus terreus* [J]. Bioelectrochemistry, 2023, 153: 108485.

[15] STADLER R, FUERBETH W, HARNEIT K, GROOTERS M, WOELLBRINK M, SAND W. First evaluation of the applicability of microbial extracellular polymeric substances for corrosion protection of metal substrates [J].

Electrochimica Acta, 2008, 54(1): 91−99.

[16] GU Ting-yu, WANG Di, LEKBACH Y, XU Da-ke. Extracellular electron transfer in microbial biocorrosion [J]. Current Opinion in Electrochemistry, 2021, 29: 100763.

[17] ZHANG Yu-xuan, LIU Hai-xian, JIN Zheng-yu, LAI Huan-sheng, LIU Hong-fang, LIU Hong-wei. Fungi corrosion of high-strength aluminum alloys with different microstructures caused by marine *Aspergillus terreus* under seawater drop [J]. Corrosion Science, 2023, 212: 110960.

[18] DAI Xin-yuan, WANG Hua, JU L, CHENG Gang, CONG Hong-bo, NEWBY B Z. Corrosion of aluminum alloy 2024 caused by *Aspergillus niger* [J]. International Biodeterioration and Biodegradation, 2016, 115: 1−10.

[19] TAN Y J, FWU Y, BHARDWAJ K. Electrochemical evaluation of under-deposit corrosion and its inhibition using the wire beam electrode method [J]. Corrosion Science, 2011, 53(4): 1254−1261.

[20] ZHANG Guo-an, YU Neng, YANG Li-ying, GUO Xing-peng. Galvanic corrosion behavior of deposit-covered and uncovered carbon steel [J]. Corrosion Science, 2014, 86: 202−212.

[21] SUAREZ E M, LEPKOVÁ K, KINSELLA B, MACHUCA SUAREZ L L. Aggressive corrosion of steel by a thermophilic microbial consortium in the presence and absence of sand [J]. International Biodeterioration & Biodegradation, 2019, 137: 137−146.

[22] YANG Jie, WANG Zheng-bin, QIAO Yan-xin, ZHENG Yu-gui. Synergistic effects of deposits and sulfate reducing bacteria on the corrosion of carbon steel [J]. Corrosion Science, 2022, 199: 110210.

[23] LIU Hai-xian, JIN Zheng-yu, WANG Zhi, LIU Hong-fang, MENG Guo-zhe, LIU Hong-wei. Corrosion inhibition of deposit-covered X80 pipeline steel in seawater containing *Pseudomonas stutzeri* [J]. Bioelectrochemistry, 2023, 149: 108279.

[24] YANG Jian-qiao, WANG Shu-zhong, LI Yan-hui, XU Dong-hai. Under-deposit corrosion of Ni-based alloy 825 and Fe−Ni based alloy 800 in supercritical water oxidation environment [J]. Corrosion Science, 2020, 167: 108493.

[25] SUAREZ E M, MACHUCA SUAREZ L L, KINSELLA B, LEPKOVÁ K. CO_2 corrosion inhibitors performance at deposit-covered carbon steel and their adsorption on different deposits [J]. Corrosion, 2019, 75(9): 1118−1127.

[26] WANG Zheng-bin, PANG Lin, ZHENG Yu-gui. A review on under-deposit corrosion of pipelines in oil and gas fields: Testing methods, corrosion mechanisms and mitigation strategies [J]. Corrosion Communications, 2022, 7: 70−81.

[27] ZHANG Yu-xuan, HE Jia-qi, ZHENG Li, JIN Zheng-yu, LIU Hai-xian, LIU Lan, GAO Zhi-zeng, MENG Guo-zhe, LIU Hong-fang, LIU Hong-wei. Corrosion of aluminum alloy 7075 induced by marine *Aspergillus terreus* with continued organic carbon starvation [J]. NPJ Materials Degradation, 2022, 6(1): 27.

[28] ZHANG B, WANG J, WU B, GUO X W, WANG Y J. CHEN D, ZHANG Y C, DU K, OGUZIE E E, MA X L. Unmasking chloride attack on the passive film of metals [J]. Nature Communications, 2018, 9(1): 2559.

[29] JI Yuan-yuan, XU Yun-ze, ZHANG Bin-bin, BEHNAMIAN Y, XIA Da-hai, HU Wen-bin. Review of micro-scale and atomic-scale corrosion mechanisms of second phases in aluminum alloys [J]. Transactions of Nonferrous Metals Society of China, 2021, 31(11): 3205−3227.

[30] ACOSTA G, VELEVA L, LÓPEZ J L, LÓPEZ-SAURI D A. Contrasting initial events of localized corrosion on surfaces of 2219-T42 and 6061-T6 aluminum alloys exposed in Caribbean seawater [J]. Transactions of Nonferrous Metals Society of China, 2019, 29(1): 34−42.

[31] LI Song-mei, ZHANG Hong-rui, LIU Jian-hua. Corrosion behavior of aluminum alloy 2024-T3 by 8-hydroxy-quinoline and its derivative in 3.5% chloride solution [J]. Transactions of Nonferrous Metals Society of China, 2007, 17(2): 318−325.

[32] WANG Ming-yang, JI Yuan-yuan, XIA Da-hai, ZHOU De-jing, ZHU Ye-sen, GAO Zhi-ming, QIN Zhen-bo, HU Wen-bin. Effect of substrate orientations on the electrochemical and localized corrosion behavior of a quad-layer Al alloy composite [J]. Journal of Materials Science & Technology, 2024, 176: 57−68.

[33] LI Zheng-yi, YU Hong-ying, SUN Dong-bai. The tribocorrosion mechanism of aluminum alloy 7075-T6 in the deep ocean [J]. Corrosion Science, 2021, 183: 109306.

[34] LIU Hong-wei, CHENG Y F. Microbial corrosion of X52 pipeline steel under soil with varied thicknesses soaked with a simulated soil solution containing sulfate-reducing bacteria and the associated galvanic coupling effect [J]. Electrochimica Acta, 2018, 266: 312−325.

[35] LIU Hong-wei, ZHONG Xian-kang, LIU Hong-fang, CHENG Y F. Microbiologically-enhanced galvanic corrosion of the steel beneath a deposit in simulated oilfield-produced water containing *Desulfotomaculum nigrificans* [J]. Electrochemistry Communications, 2018, 90: 1−5.

[36] SUN Qing, YANG Ming, JIANG Yun, LEI Lei, ZHANG Yan. Achieving excellent corrosion resistance properties of 7075 Al alloy via ultrasonic surface rolling treatment [J]. Journal of Alloys and Compounds, 2022, 911: 165009.

[37] QI Xing, JIANG Bo, SONG Ren-guo. Effects of ageing treatment on corrosion behavior of 7075 aluminum alloy coated by micro arc oxidation (MAO) [J]. Corrosion Science, 2022, 199: 110164.

[38] SLIEM M H, FAYYAD E M, ABDULLAH A M, YOUNAN N A, AL-QAHTANI N, NABHAN F F, RAMESH A, LAYCOCK N, RYAN M P, MAQBOOL M, ARORA D. Monitoring of under deposit corrosion for the oil and gas industry: A review [J]. Journal of Petroleum Science and Engineering, 2021, 204: 108752.

[39] WANG Qiu-yu, WU Wei, LI Qing, ZHANG De-ping, YU Yi-fan, CAO Bei, LIU Zhi-yong. Under-deposit corrosion of tubing served for injection and production wells of CO_2 flooding [J]. Engineering Failure Analysis, 2021, 127: 105540.

[40] MAHIDASHTI Z, REZAEI M, ASFIA M P. Internal under-deposit corrosion of X60 pipeline steel upon installation in a chloride-containing soil environment [J]. Colloids and Surfaces A: Physicochemical and Engineering Aspects, 2020, 602: 125120.

[41] DENG Chen-man, XIA Da-hai, ZHANG Rui-feng, BEHNAMIAN Y, HU Wen-bin, BIRBILIS N. On the localized corrosion of AA5083 in a simulated dynamic

seawater/air interface—Part 2: Effects of wetting time [J]. Corrosion Science, 2023, 221: 111367.

[42] ZHANG Guo-an, CHENG Y F. Localized corrosion of carbon steel in a CO_2-saturated oilfield formation water [J]. Electrochimica Acta, 2011, 56(3): 1676−1685.

[43] XIA Da-hai, JI Yuan-yuan, ZHANG Rui-feng, MAO Ying-chang, BEHNAMIAN Y, HU Wen-bin, BIRBILIS N. On the localized corrosion of AA5083 in a simulated dynamic seawater/air interface—Part 1: Corrosion initiation mechanism [J]. Corrosion Science, 2023, 213: 110985.

[44] HE Jia-qi, TAN Yu, LIU Hai-xian, JIN Zheng-yu, ZHANG Yu-xuan. HE Fei-xiang, YAN Zhi-xiang, LIU Hong-fang, MENG Guo-zhe, LIU Hong-wei. Extracellular polymeric substances secreted by marine fungus *Aspergillus terreus*: Full characterization and detailed effects on aluminum alloy corrosion [J]. Corrosion Science, 2022, 209: 110703.

[45] MIEČINSKAS P, LEINARTAS K, UKSIENĖ V, JUZELIŪNAS E. QCM study of microbiological activity during long-term exposure to atmosphere — Aluminium colonisation by *Aspergillus niger* [J]. Journal of Solid State Electrochemistry, 2007, 11: 909−913.

[46] WANG Jun-lei, XIONG Fu-ping, LIU Hong-wei, ZHANG Tian-sui, LI Yan-yan, LI Chen-jing, XIA Wu, WANG Hai-tao, LIU Hong-fang. Study of the corrosion behavior of *Aspergillus niger* on 7075-T6 aluminum alloy in a high salinity environment [J]. Bioelectrochemistry, 2019, 129: 10−17.

[47] JIRÓN-LAZOS U, CORVO F, DE LA ROSA-GARCÍA, S C, GARCÍA-OCHOA E M, BASTIDAS D M, BASTIDAS J M. Localized corrosion of aluminum alloy 6061 in the presence of *Aspergillus niger* [J]. International Biodeterioration and Biodegradation, 2018, 133: 17−25.

[48] AL-SHAMARI A R, AL-MITHIN A W, OLABISI O, MATHEW A. Developing a metric for microbilogically influenced corrosion (MIC) in oilfield water handling systems [C]//Corrosion 2013. Orlando: NACE International, 2013.

[49] JI Yuan-yuan, HU Qian, XIA Da-hai, LUO Jing-li. Corrosion susceptibility of passive films on 1060, 2024, and 5083 aluminum alloys: Experimental study and first-principles calculations [J]. Journal of the Electrochemical Society, 2023, 170(4): 041505.

海洋环境中沉积物覆盖下 7075 铝合金的真菌腐蚀行为和机制

王佳平[1]，张 怡[2]，刘宏伟[1]，尹衍升[2]

1. 中山大学 化学工程与技术学院，珠海 519082；
2. 广州航海学院 海洋严酷环境使役材料与运维装备广东省高校重点实验室，广州 510725

摘 要：系统研究了模拟海水环境中由土曲霉引起的沉积物覆盖下 7075 铝合金的腐蚀行为，旨在为海洋环境中由真菌导致的沉积物下铝合金的腐蚀机制研究提供一些新的思路。电化学阻抗谱、极化曲线、丝束电极以及表面分析手段获得的研究结果表明，土曲霉可以在沉积物下存活，但其活性较差，其固着孢子数随着沉积物厚度的增加而减少。铝合金的均匀腐蚀和点蚀在土曲霉存在条件下都明显加速，沉积物下 7075 铝合金的点蚀源自于小阳极和大阴极组成的电偶电池的形成，且沉积物对铝合金的腐蚀有抑制效果。裸试样和沉积物覆盖下试样之间的电偶效应在土曲霉存在条件下明显增强。

关键词：真菌腐蚀；沉积物下腐蚀；点蚀；土曲霉；7075 铝合金

(Edited by Wei-ping CHEN)